Applied Physics A (2021) 127:46
https://doi.org/10.1007/s00339-020-04173-2

Applied Physics A
Materials Science & Processing

Statistical analysis of current–voltage characteristics in Au/Ta_2O_5/n-GaN Schottky barrier heterojunction using different methods

V. Manjunath[1] · Nanda Kumar Reddy Nallabala[2] · C. Yuvaraj[3] · Chandramohan Kukkambakam[4] · Venkata Krishnaiah Kummara[5] · Suresh Kumar[6] · Shivani Sharma[6] · M. V. Lakshmaiah[7] · Vasudeva Reddy Minnam Reddy[8]

Received: 26 September 2020 / Accepted: 25 November 2020 / Published online: 3 January 2021

Abstract

We report on the influence of incorporation of Ta_2O_5 thin film at the interface of Au/GaN by means of e-beam evaporation technique. The fabricated Au/Ta_2O_5/n-GaN MIS junctions have been analysed using *I–V* measurements and were extended to a voltage range of ± 20 V. The Schottky diode parameters for instance Φ_{bo}, *n* and R_S values are evaluated using *I–V* curves at room temperature. The statistical distribution analysis provides the mean 'Φ_{bo}' value of 0.85 eV with deviation of 0.00181 eV and mean value from '*n*' is 1.36 with a normal deviation of 0.00562. Two important electrical parameters such as R_S and R_{sh} values are also extracted from *I–V* characteristics. Furthermore, Cheung, Norde, modified Norde, Hernandez and Chattopadhyay methods are used to evaluate the Schottky barrier parameters from *I–V* data. The comparison is made between the extracted electrical parameters such as *n*, Φ_{bo} and R_S from *I–V* characteristics of Au/Ta_2O_5/n-GaN MIS junctions and are in well agreement with each other. Under forward-bias, the fabricated Au/Ta_2O_5/n-GaN MIS junction conduction mechanisms such as ohmic and SCL were found to be dominant at lower and higher voltage regimes, respectively. By fitting reverse-bias region of *I–V* curves, PF conduction mechanism was found to be dominant at the interfaces of Au/Ta_2O_5/n-GaN. In conclusion, the obtained superior rectification ratio of 6.06×10^4 and higher SBH of 0.87 eV was ascribed to the purposefully deposited undoped GaN buffer layer between epitaxial GaN and sapphire substrate.

Keywords Ideality factor · Ta_2O_5 interfacial layer · Series/shunt resistance · Gallium nitride · Schottky barrier height

✉ Nanda Kumar Reddy Nallabala
nandasvu@gmail.com

✉ Vasudeva Reddy Minnam Reddy
drmvasudr9@gmail.com

[1] Department of Physics, Sri Padmavati Mahila Visvavidyalayam, Tirupati, Andhra Pradesh 517502, India

[2] Department of Physics, Madanapalle Institute of Technology and Science, Madanapalle, Andhra Pradesh 517325, India

[3] Department of Mechanical Engineering, Madanapalle Institute of Technology & Science, Madanapalle, Andhra Pradesh 517325, India

[4] Department of Chemistry, Madanapalle Institute of Technology and Science, Madanapalle, Andhra Pradesh 517325, India

[5] Department of Physics, Rajeev Gandhi Memorial College of Engineering and Technology, Nandyal 518501, Andhra Pradesh, India

[6] Department of Electronic Science, Kurukshetra University, Kurukshetra 136119, India

[7] Department of Physics, Sri Krishnadevaraya University, Anantapur, Andhra Pradesh, India

[8] School of Chemical Engineering, Yeungnam University, Gyeongsan 38541, Republic of Korea

1 Introduction

Presently, wide-bandgap semiconductors (WBGSs) such as AlN, InN and GaN are broadly used in device fabrication which includes applications of short wavelength range optoelectronic, high-frequency/power electronic devices. This was accomplished due to their higher intrinsic material properties of WBGSs compared to conventional semiconductors such as Si and GaAs as indicated in Table 1 [1–3]. Among these WBG materials, gallium nitride (GaN) has the potential in terms of good optical/electrical properties, high carrier mobility, strong ultraviolet absorption, high chemical resistivity, direct bandgap, good thermal conductivity and high melting points [1–7]. These aforesaid properties cause GaN to be used in diverse important applications such as sensors, light-emitting diodes, metal–semiconductor field effect transistors (MSFETs), high electron mobility transistors (HEMTs), heterostructure field effect transistors (HFETs) and photocatalysts [8–15]. As GaN-based metal/semiconductor junction (MSJ)-based Schottky barrier diodes (SBDs) are vital in almost all electronic devices, analysis of electronic properties/current transport at the MSJ interfaces requires further analysis on reliable and stable ohmic/Schottky contacts. Current–voltage (*I–V*) features of MSJs give an enormous information on electrical and physical assets of a bulk material of semiconductor and its interface. The MSJ-based devices may be affected by low breakdown voltage and high leakage current, which bounds the device performance, stability and reliability. One can overcome this limitation by retaining a thin high-k dielectric oxide layer at the interface of MSJ. This deliberately deposited high-*k* interlayer has remarkable advantages such as greater rectification ratio, lower leakage current, lower ideality factor (n), higher Schottky barrier height (SBH:Φ_{bo}) and good thermal stability. Also, the MIS junction characteristic depends on the interface states, interlayer homogeneity and series resistance (R_S). The vital limitations of existing conventional gate dielectric materials such as silicon dioxide (SiO_2) are prone to higher gate leakage currents, thus, the search for materials with advanced high-*k* dielectric constant to permit further reduction in the gate leakage currents in the real time device applications.

Developments in shrinking the size of integrated circuits (ICs) to improve the logical density and performance of chips necessitates the substitution of copper (Cu) for aluminium (Al) as interconnections in silicon-based ICs. This is due to the fact that Cu offers lower resistivity, superior electromigration and stress-voiding resistance compared to Al and its alloys [16]. Still, Cu limits its usage owing to its high mobility/reactivity and poor adhesiveness, which should be elucidated first prior to its practical usage in ICs. Novel materials that act as effective diffusion barrier and adhesion promoters between Cu and underlying substrate are essential. Materials such as tantalum (Ta), tantalum nitride (TaN) and tantalum carbide (TaC) thin films are already proven as the utmost capable diffusion barriers and were used to prevent diffusion/reaction of Cu with the underlying silicon and adjoining SiO_2 dielectrics [17–19]. Thus, the above-said superior electrical, structural and thermal stability characteristics of Ta, TaC, TaN found applications as renowned diffusion barriers in electronic devices [20] and X-ray lithography [21–23]. On the other hand, tantalum pentoxide (Ta_2O_5) became an attractive material due to its high-k dielectric property and found applications in anti-reflective coatings, photocatalysts and resistance-change random access memory (ReRAM) [24–26]. Many other research groups have explored the fabrication of Ta_2O_5 as an interfacial oxide layer at the MS interface and tested their electrical characteristics by diverse deposition methods [27–32]. For example, Yu et al. [27] and Joo et al. [28] reported that Pt/Ta_2O_5/SiC and Pd/Ta_2O_5/SiC MIS type SBD structures could be used in hydrogen gas sensing applications. Lakshmi et al. [29] investigated Au/Ta_2O_5/n-GaN MIS structure and studied its electrical properties at different annealing temperatures. They concluded that the annealed samples exhibited betterment in electrical properties due to the reduction of interface states density. Alimardani et al. [30] fabricated Nb_2O_5- and Ta_2O_5-based MIS structures by means of atomic layer deposition technique and they reported that the dominant conduction mechanism at smaller biases was Schottky emission whereas at higher biases it was Frenkel–Poole (PF) emission. Reddy et al. [31] investigated Al/Ta_2O_5/p-Si MIS SBD with Ta_2O_5 as the insulating layer and reported higher SBH for the prepared devices compared to Al/p-Si MS SBD. Kumar et al. [32] fabricated Ni/n-GaN SBDs and reported current transport properties using different methods.

In MIS junction, the traditional thermionic emission (TE) theory is not sufficient to describe the charge or carrier transport mechanism through the intentionally deposited interfacial interlayer [33, 34]. As the SBH is often influencing the current transport at the interfaces of MIS structure, we

Table 1 Material properties of Si, GaAs, 4H–SiC and GaN for comparison

Parameter	Si	GaAs	4H–SiC	GaN
E_g (eV)	1.12	1.42	3.25	3.40
E_C (MV/cm)	0.3	0.4	3.0	4.0
μ_n ($cm^2V^{-1}S^{-1}$)	1500	8500	1000	1250
ε	11.8	12.8	9.7	9.0
V_{sat} (10^7 cm/s)	1	2	2	2.5
λ ($W.cm^{-1}.K^{-1}$)	1.5	0.5	4.9	2.3

E_g bandgap; E_C critical electric field; μ_n electron mobility; ε dielectric constant; V_{sat} saturation electron velocity; λ thermal conductivity

extended our analysis of electrical parameters by TE theory with different methods. This can allow one to understand better about the SBH (Φ_{bo}), n, R_S and current conduction mechanisms, which are highly crucial for the technology of advanced device fabrication. The key significance of the present manuscript is to describe the electronic parameters using different fitting methods using experimentally measured I–V data of Au/Ta_2O_5/n-GaN MIS SBD in the ± 20 V range at room temperature. As high work function metal gold (Au) is used as a Schottky contact and Al/Ti is used as ohmic contact, we have obtained a very good rectification. Also, we have used UV–Visible, AFM and XRD techniques to check the Ta_2O_5 oxide layer bandgap, surface morphology and crystallinity of Al/Ti/GaN structure, respectively.

2 Materials and methods

Si-doped n-type GaN epitaxial layer with 4.5 µm thickness was grown on undoped GaN buffer layer of thickness ~ 50 nm, which confined on sapphire (0001) substrate using metal organic chemical vapour deposition (MOCVD). Estimated carrier concentration of the n-type GaN epitaxial layer was found to be $1–3 \times 10^{17}$ cm^{-3}. Prior to the deposition of metals and oxide, n-GaN sample was undergone with cleaning procedure steps reported in our previous work [35]. By an electron beam (e-beam) evaporation system, Ti/Al (30 nm/60 nm) was deposited onto half portion of 5 mm size of n-GaN with dots of 0.003 cm diameter. Then samples were annealed at 650 ℃ for 60 s in N_2 gas to yield better adhesive ohmic contact to n-GaN. Subsequently, the Ta_2O_5 of purity 99.9% (~ 35 nm thick) material which is in pellet form was deposited on other half portion (2.5 mm) of the n-GaN substrate. Then Au (70 nm) metal of purity 99.99% was deposited on Ta_2O_5 film using e-beam evaporation system using 0.03 mm diameter stainless steel mask. The schematic of the fabricated Au/Ta_2O_5/n-GaN MIS SBD heterojunction is shown in Fig. 1. Deposited Au and Ta_2O_5 film thickness was evaluated by quartz crystal microbalance at a pressure of $3–5 \times 10^{-5}$ mbar. UV–Vis technique (Shimadzu, UV-1800, Japan) was employed to evaluate the direct optical bandgap of the Ta_2O_5 material. Atomic force microscopy (AFM: A.P.E. Research, Italy) analysis was employed to distinguish the surface morphology/contact quality of Ta_2O_5 on to GaN. X-ray diffraction (Panalytical XPRT Pro) technique was used to check the interfacial reaction between Ti/Al and GaN. The I–V characteristic properties of the prepared Au/Ta_2O_5/n-GaN MIS junction were studied by 2450 model Keithley source. Finally, using different methods, the Schottky diode parameters were interpreted with the help of the conduction mechanisms such as ohmic, space charge limited (SCL), Schottky emission (SE) and Poole–Frenkel (PF) at 300 K, respectively.

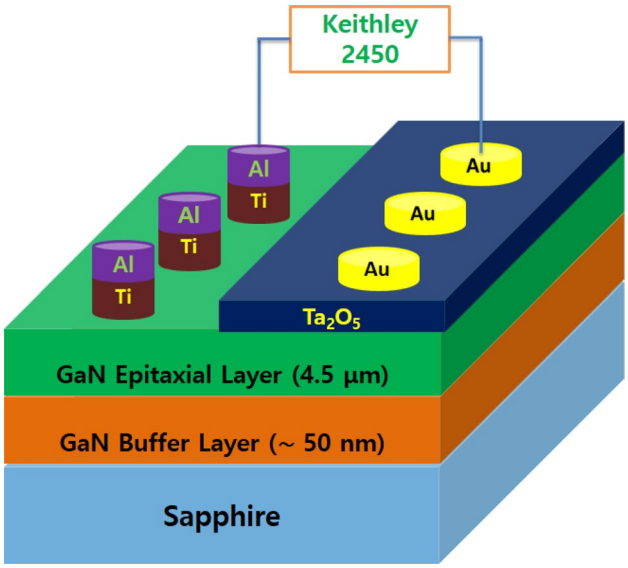

Fig. 1 Schematic diagram of the fabricated Au/Ta_2O_5/n-GaN MIS SBD

3 Results and discussion

As thin film growth mechanism is influencing the electrical, optical and structural properties of the fabricated device performance or functionality, surface topography has been employed to analyse the Ta_2O_5 films. Generally, topographical information is acquired using AFM in non-contact mode which is being the utmost preferred compared to the other techniques due to its versatility. Figure 2a, b displays the two and three-dimensional surface morphologies of Ta_2O_5 films made on n-type GaN using non-contact mode AFM with scan area of 1 μm^2. It indicates the formation of smooth and continuous surface morphology with root-mean square roughness of 2.80 nm. As shown in Fig. 2b, the formed Ta_2O_5 films deposited by means of e-beam evaporation revealed gathering of atomic clusters or island. Similar surface morphology was observed for Ta_2O_5 films in the case of ion-assisted e-beam evaporation [36] and e-beam evaporation [37] techniques.

To understand the electronic structure with the help of optical bandgap of Ta_2O_5 films, UV–Vis absorption spectral study was employed. In general, the absorption arises as of electronic transitions related within the Ta_2O_5 material. The UV–Vis spectrum for the as-deposited Ta_2O_5 films on quartz is shown in the inset of Fig. 3. As can be seen from the inset of Fig. 3, the maximum absorption for Ta_2O_5 film was observed to take place below 400 nm with a sharp absorbance peak noticed at 295 nm. Direct optical bandgap of the as-deposited Ta_2O_5 thin films was evaluated using Tauc's plot. As shown in Fig. 3, the consequent Tauc's plot is used for the estimation of the direct optical

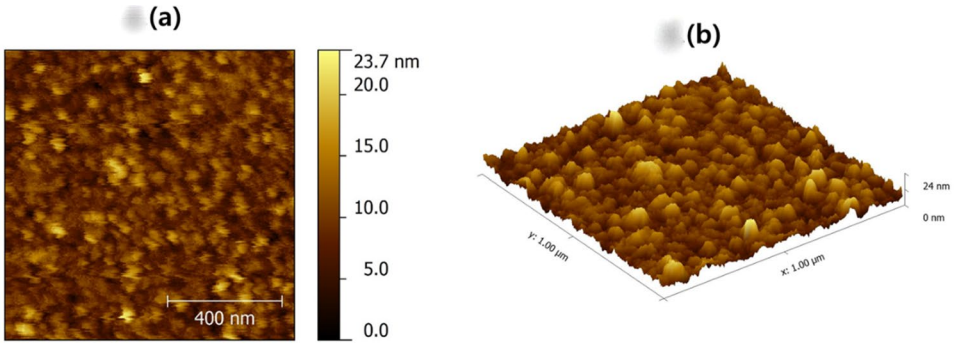

Fig.2 The top view of **a** 2D **b** 3D AFM surface morphology of the as-prepared Ta_2O_5 film on n-GaN

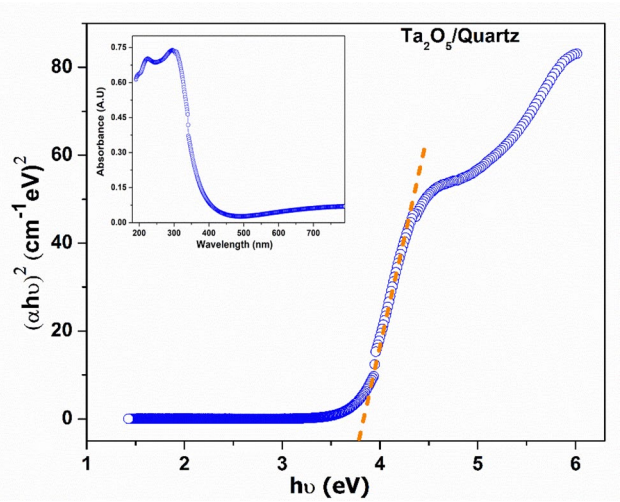

Fig. 3 UV–Vis absorption spectra of as-prepared Ta_2O_5 films (shown in inset) and Tauc's plot of $(\alpha h\nu)^2$ versus $h\nu$

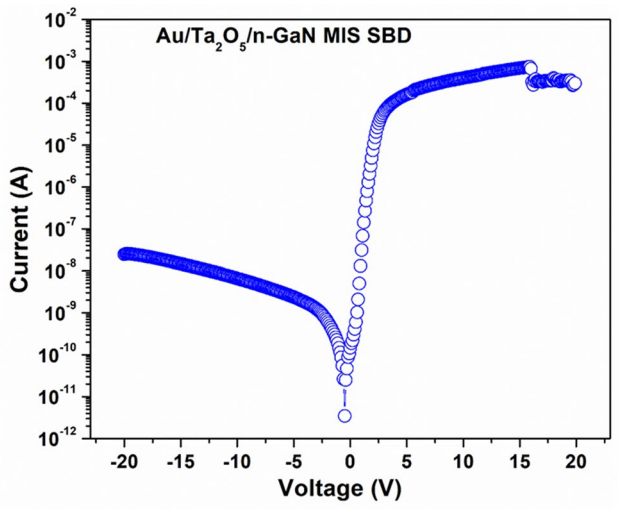

Fig. 4 Forward and reverse ln (I)–V characteristics of Au/Ta_2O_5/n-GaN MIS junction measured at room temperature in the voltage range ± 20 V

bandgap energy 'E_g' by extrapolation of the $(\alpha h\nu)^2$ versus '$h\nu$' curve to zero absorption and can be written as [38]

$$\alpha h\gamma = E_D(h\gamma - E_g)^{1/2}, \tag{1}$$

where α is absorption coefficient, E_D is constant and '$h\nu$' is photon energy.

The evaluated direct optical bandgap energy of 3.85 eV estimated for the as-deposited Ta_2O_5 film in the present work is in well accordance with the earlier reported value of 3.9 eV in the case of e-beam evaporated as-deposited Ta_2O_5 films [37].

The Au/Ta_2O_5/n-GaN MIS junction showed a good rectification as shown in Fig. 4 with a reverse leakage current of 6.4×10^{-10} A at − 2 V. This result designates the reduction of leakage current due to the intentionally introduced Ta_2O_5 interlayer at the interface of Au and n-GaN. The basic electrical parameters of the Au/Ta_2O_5/n-GaN MIS SBD can be derived using TE theory. The forward bias I–V relation can be written according to TE theory [39, 40].

$$I = AA^*T^2\exp\left(-\frac{q\Phi_{bo}}{kT}\right)\left[\exp\left(\frac{q(V-IR_S)}{nkT}\right)-1\right]. \tag{2}$$

In Eq. (2), I_o is the reverse-saturation current determined from ln (I)–V plot at $V=0$ and A^* is the Richardson constant [35] (26.4 Acm^{-2} K^{-2} for n-type GaN). As can be seen in Fig. 4, the ln (I)–V plot for Au/Ta_2O_5/n-GaN MIS SBD in the voltage range of ± 20 V displayed a good rectification ratio. The rectification ratio (RR), i.e. the ratio of forward current (4×10^{-4} A) to reverse current (6.59×10^{-9} A) at 10 V bias was found to be 6.06×10^4. This ensures that the fabricated MIS junction is exhibiting superior RR due to the formations of good Schottky (Au) and ohmic (Ti/Al) contacts. To check the quality of the fabricated Al/Ti ohmic contact to GaN, we have employed X-ray diffraction study with a 2θ scan in the range of 20–80°. Figure 5 illustrates the grazing-incidence X-ray diffraction (GIXRD) scan of the Al/Ti/GaN sample annealed at 650 °C in N_2 atmosphere for a period of one minute. The peaks found at $2\theta=22.6$, 26.4, 29.05, 31.5, 39.1, 45.5 and 65.4° correspond to Ti–Al

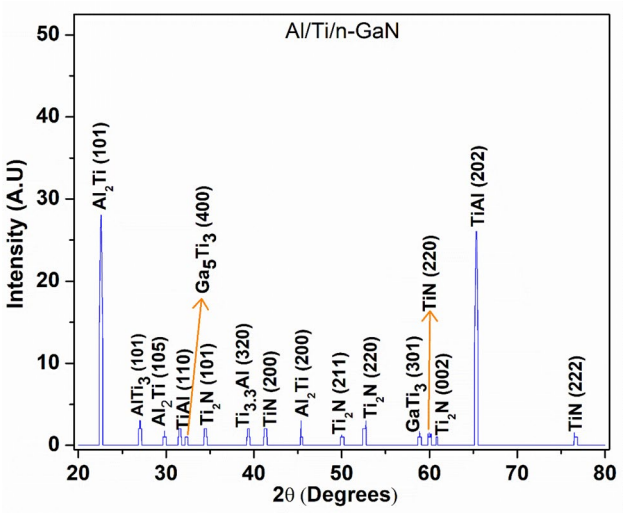

Fig. 5 XRD plot of Al/Ti/n-GaN structure annealed at 650 °C for 1 min in N_2 ambient

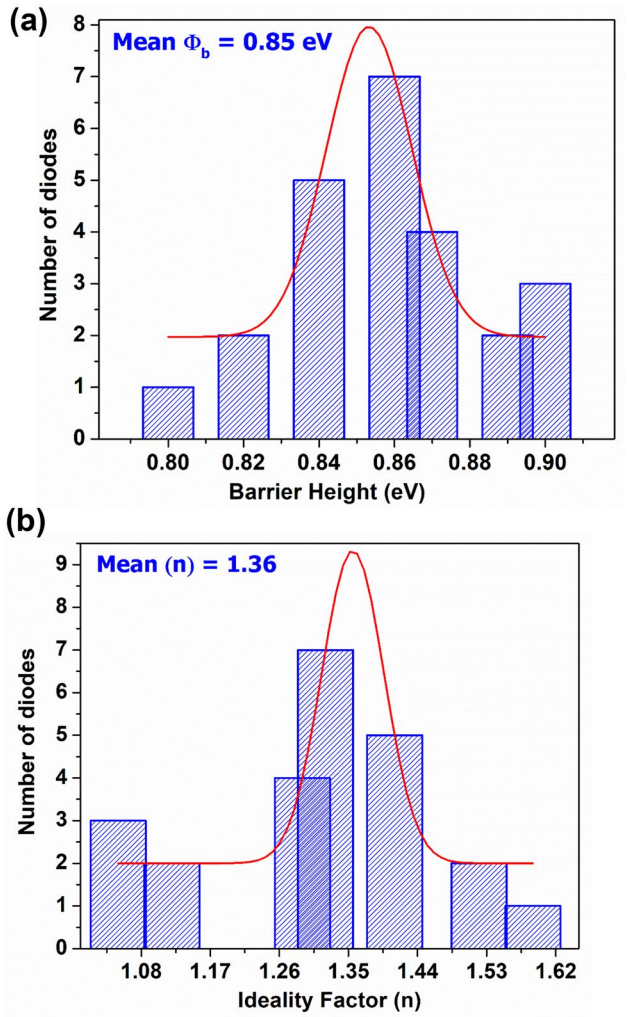

Fig. 6 **a** Gaussian distribution of Schottky barrier heights and **b** ideality factors calculated from the forward bias *I–V* characteristics for Au/Ta_2O_5/n-GaN MIS junction

alloys of Al_2Ti (101), $AlTi_3$ (101), Al_2Ti (105), TiAl (110), $Ti_{3.3}Al$ (320), Al_2Ti (200) and TiAl (202), respectively. The two peaks originated at $2\theta = 32°$ and 59.1° corresponds to Ga-Ti phases of Ga_5Ti_3 (400) and $GaTi_3$ (301), respectively. Furthermore, Ti–N phases of Ti_2N (101), TiN (200), Ti_2N (211), Ti_2N (220), TiN (220), Ti_2N (002) and TiN (222) found at $2\theta = 34.5$, 41, 50.2, 52.3, 60.2, 61 and 76.3°, respectively. Most of the above-said Ti–N and Ti–Al phases were already reported in previous works [41–44]. The presence of Ti–N and Ti–Al phases in the X-ray diffractogram of Al/Ti metallization point out the development of good quality ohmic contacts to n-GaN. Thus, the formation of these desired Ti–N compound and low resistance inter-metallic Ti–Al phases are crucial in obtaining the superior quality ohmic contact, confirming the creation of N vacancies at the MS interface which intern enhances the tunnelling current ensuring the formation of good ohmic contact to n-GaN [45–47].

The SBH (Φ_{bo}) is calculated by means of Eq. (3) and the slope of the ln (*I*)–*V* characteristics yields the ideality factor (*n*) value that are attained from the following equation:

$$\Phi_{bo} = \frac{kT}{q}\ln\left(\frac{AA^*T^2}{I_0}\right), \tag{3}$$

$$n = \frac{q}{kT}\frac{dV}{d(\ln I)}. \tag{4}$$

We fabricated the sixteen number of Au/Ta_2O_5/n-GaN MIS SBD heterojunction dots/devices on the same GaN semiconductor. The 'Φ_{bo}' and '*n*' values are calculated from the distinct *I–V* plots (± 20 V). The diodes SBH (Φ_{bo}) values varied from 0.80 to 0.90 eV and the '*n*' values ranged from 1.05 to 1.59. From the results, it is clear that the identically prepared MIS junction 'Φ_{bo}' and '*n*' values slightly varied from diode to diode. These results indicated that the potential barriers at the interfaces of MIS SBD strongly depend on the Ta_2O_5 interlayer between metal and semiconductor as well as applied voltage that is expected by the image-force effect. Figure 6a, b shows the statistical distribution analysis of the 'Φ_{bo}' and '*n*' values for the sixteen Au/Ta_2O_5/n-GaN MIS junctions from *I–V* plot with the voltage range of ± 20 V, at room temperature. The calculated 'Φ_{bo}' and '*n*' values are experimentally fitted by Gaussian distribution functions. The statistical analysis yields an average 'Φ_{bo}' value of 0.85 eV with normal deviation of 0.00181 eV and average '*n*' of 1.36 with a normal deviation of 0.00562 for the Ta_2O_5-based MIS SBD. The calculated '*n*' is larger than unity and the reason for this can be ascribed to the facts such as the distribution

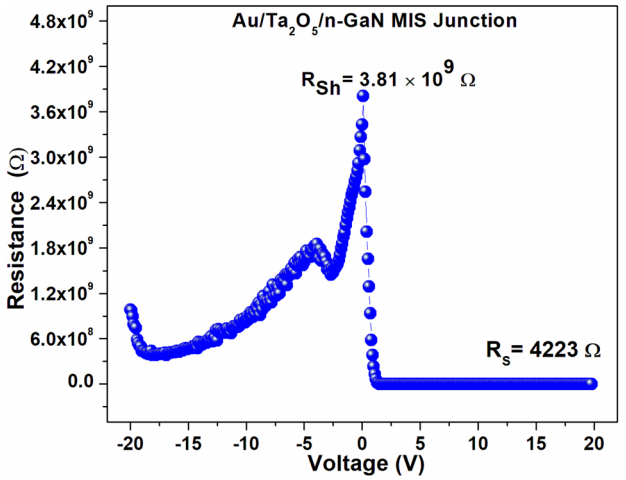

Fig. 7 Junction resistance versus voltage for the Au/Ta_2O_5/n-GaN MIS junction at room temperature

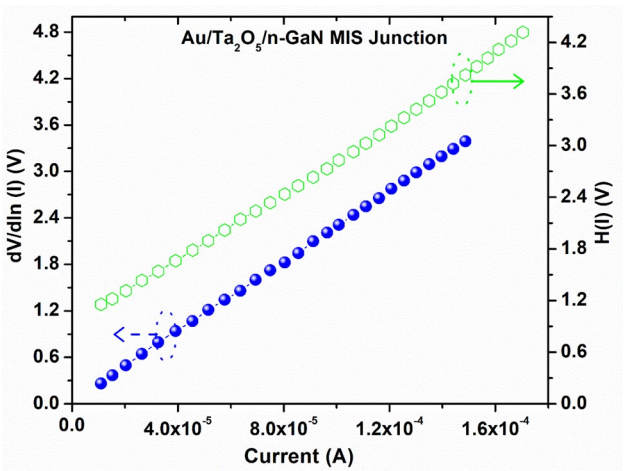

Fig. 8 Plot of d*V*/dln (*I*) and H (*I*) versus I for the Au/Ta_2O_5/n-GaN MIS junction

of the interface states, recombination-generation/tunnelling process and image-force effects [48].

The shunt resistance (R_{Sh}) and series resistance (R_S) are the other two important electrical parameters to be evaluated for the Au/Ta_2O_5/n-GaN MIS SBD. These values are extracted using the expression $R_j = \partial V/\partial I$ from *I–V* analysis at room temperature and is shown in Fig. 7. Generally, in the case of ideal device, the R_S and R_{Sh} should be close to zero and infinity, respectively [49]. From Fig. 7, the R_S and R_{Sh} values are evaluated as 4.2 kΩ and 3.81 GΩ, respectively. These higher values of R_S and R_{Sh} may be due to the deliberately deposited Ta_2O_5 interlayer/interface states density (N_{SS}) at the MS interface. Also, the R_S and N_{SS} are essential parameters in MIS SBDs, which affect the linearity of the *I–V* characteristics, when the applied voltage is effectively high as shown in Fig. 4. The R_S is significant in the non-linear curve region at the high applied voltage in the forward bias *I–V* characteristics. The main parameters such as '*n*' and R_S can also be evaluated by Cheung and Cheung method [50]. The Cheung's function can be written as

$$\frac{dV}{d(\ln I)} = IR_s + n\left(\frac{kT}{q}\right), \tag{5}$$

$$H(I) = V - \left(\frac{nkT}{q}\right)\ln\left(\frac{I}{AA^*T^2}\right), \tag{6}$$

and *H* (*I*) is represented as

$$H(I) = n\Phi_{bo} + IR_s. \tag{7}$$

The d*V*/d(ln *I*) versus *I* curve for Au/Ta_2O_5/n-GaN MIS SBD is illustrated in Fig. 8. The plot should produce a straight line for the non-linear section of forward bias *I–V* characteristics. The 'R_S' and '*n*' values are calculated from slope and intercept of the plot as shown in Fig. 8. The extracted R_S and '*n*' values for Au/Ta_2O_5/n-GaN MIS SBD are 22.6 kΩ and 1.30, respectively. The *H* (*I*) versus *I* plot for Au/Ta_2O_5/n-GaN MIS SBD at 300 K is also shown in Fig. 8. According to Eq. (7), Fig. 8 also be a straight line with intercept (*y*-axis) equal to Φ_b results. The calculated Φ_b and R_S values were 0.88 eV and 19.7 kΩ, respectively. The R_S values acquired from *H* (*I*) versus *I* plot are consistent with the d*V*/d(ln *I*) plot which signifies the reliability of the Cheung's methodology.

To calculate consistent Φ_{bo} and R_S values of Au/Ta_2O_5/n-GaN MIS SBD, an alternate method was developed by Norde and Bohlin [51, 52]. Usually, the *n* values lie in between 1 and 2; the function F (*V*) can be expressed as

$$F(V) = \frac{V}{2} - \frac{KT}{q}\ln\left(\frac{I(V)}{AA^*T^2}\right). \tag{8}$$

The current (I_o) corresponds to minimum of F (*V*) versus *V* plot and R_S can be extracted using [39]

$$R_S = \frac{kT}{qI_o}, \tag{9}$$

and Φ_b can be extracted using

$$\Phi_{bo} = F(V_{min}) + \frac{V_{min}}{2} - \frac{KT}{q}, \tag{10}$$

where F (V_{min}) and V_{min} are the values of F (*V*) and *V* conforming to the least current (I_o) values. The modified Norde function can be written as [39]

$$F(V) = \frac{V}{\gamma} - \frac{KT}{q}\ln\left(\frac{I(V)}{AA^*T^2}\right). \tag{11}$$

Meanwhile, the 'n' value lies between 1 and 2; therefore, $\gamma=2$ (>1). Then the Φ_b and R_S values are calculated using the following equations [39]:

$$Rs = \frac{kT(\gamma - n)}{qI_{min}}, \tag{12}$$

$$\Phi_{bo} = F(V_{min}) + \frac{V_{min}}{\gamma} - \frac{kT}{q}. \tag{13}$$

The F (V) versus V plot for the fabricated Au/Ta_2O_5/n-GaN MIS SBD is shown in Fig. 9. The estimated Φ_{bo} and R_S values are 0.85 eV and 96 MΩ. The calculated Φ_{bo} values from the Norde method demonstrate good agreement with the Φ_{bo} value calculated using I–V method. But the calculated R_S values from Norde method are higher compared to the Cheung's function. This is owing to the fact that the Cheung's method is applied only to the non-linear region of I–V characteristics whereas in Norde method, the fitting is made to the entire forward bias region of the I–V curves of the fabricated MIS SBD.

To calculate 'n' and 'Φ_{bo}' values, a new method was developed by Hernandez et al. [53] from the homogeneous non-ideal I–V plot. Voltage-dependent properties of the 'n' and Φ_b can be conveyed with a voltage-dependent function as [39]

$$Z(V,T)_i = \frac{kT}{q}\left[\ln\left(\frac{I_i}{AA^*T^2\left[1-\exp\left(-qV_d/kT\right)\right]}\right)\right] \tag{14}$$

$$\text{and} Z(V,T)_i = -\Phi_{bo}(V,T)_i + \frac{V_d}{n_o(V,T)_i}. \tag{15}$$

Using Fig. 10, the voltage-dependent 'n' and Φ_b values were calculated as 1.32 and 0.89 eV, respectively.

For huge values of R_S and interface state densities (N_{SS}), the logarithmic I–V plot becomes non-linear as shown in Fig. 4. This factor limits the evaluation of saturation current (I_o) from fitting; hence, the calculated values of Φ_{bo} using I_o are not reliable. To avoid this limitation, Chattopadhyay [54] developed a model to evaluate the surface potential (Ψ_S) and it can be expressed as

$$\Psi_S = \frac{kT}{q}\ln\left(\frac{AA^*T^2}{I}\right) - Vn. \tag{16}$$

Using this method, Φ_{bo} and n values can be evaluated from [29, 55]

$$\Phi_{bo} = \Psi_S(I_C, V_C) + C_2V_C + V_n. \tag{17}$$

$$C_2 = \frac{1}{n} = -\left(\frac{d\Psi_S}{dV}\right)_{I_C,V_C}. \tag{18}$$

Using Eqs. (17) and (18), the 'Φ_{bo}', 'n' values of the MIS SBD were found to be 0.82 eV and 1.28, respectively. 'Φ_{bo}' and 'n' values attained from the Ψ_S versus V plot (Fig. 11) were consistent with those calculated from the forward-bias (I–V) and $Z(V, T)_i$ versus V plots of the prepared Au/Ta_2O_5/n-GaN MIS SBD. Thus, consequently, the methods employed here have shown effective and good consistence with each other. The reason for this can be ascribed to the insertion of Ta_2O_5 oxide layer at the MS

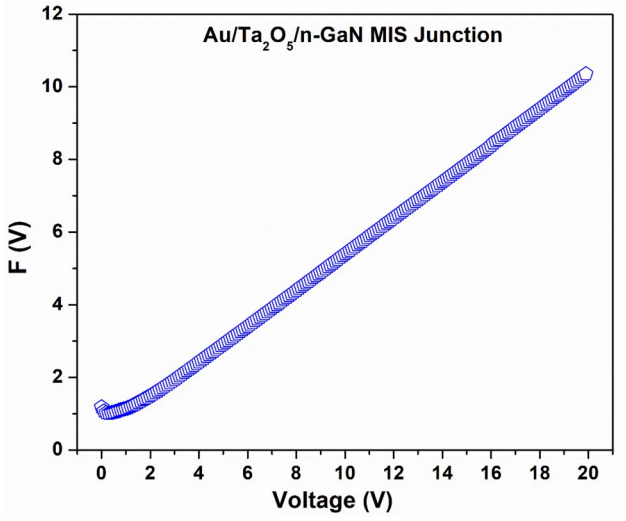

Fig. 9 Modified F (V) versus V plot for the Au/Ta_2O_5/n-GaN MIS junction

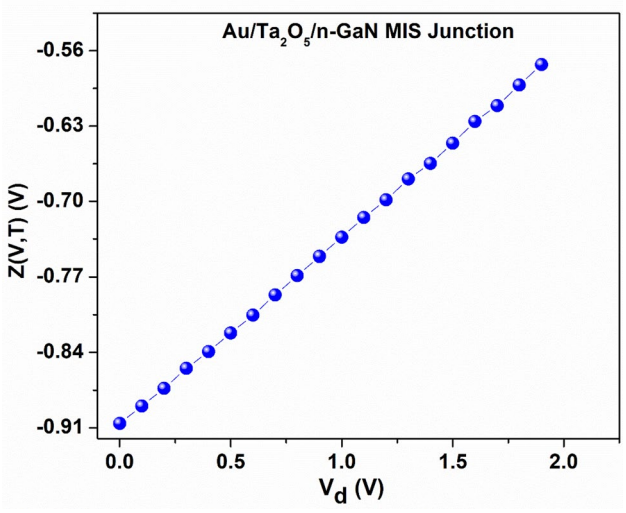

Fig. 10 The plot of $Z(V, T)_i$ versus V_d for the Au/Ta_2O_5/n-GaN MIS junction

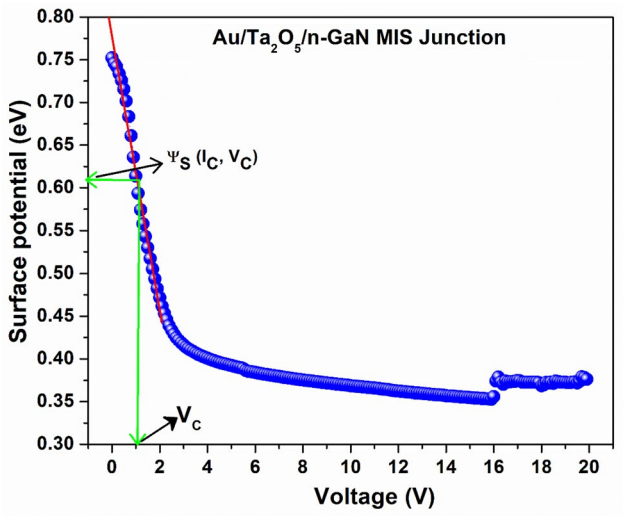

Fig. 11 Surface potential versus forward bias voltage characteristics of the Au/Ta_2O_5/n-GaN MIS junction

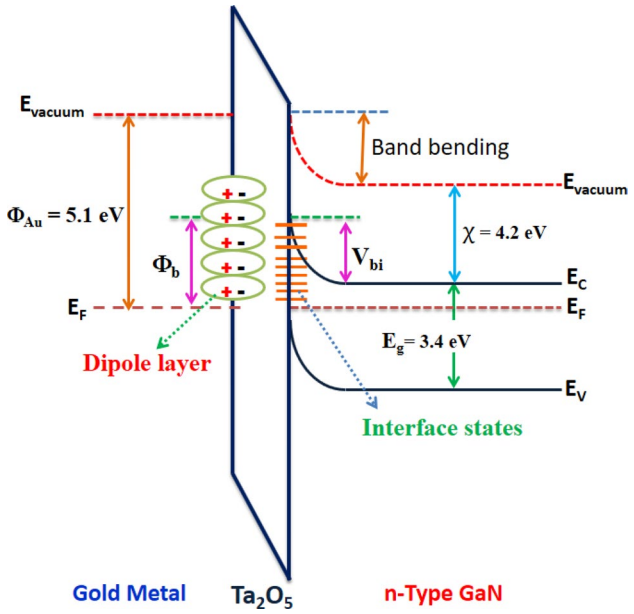

Fig. 12 Energy band diagram of Au/Ta_2O_5/n-GaN MIS junction

interface. Figure 12 elucidates the energy level band diagram of the Au/Ta_2O_5/n-GaN MIS junctions with interfacial layer indicating work function of Au metal, electron affinity/energy gap of GaN and the resulting band bending after the contact has been made. As can be seen from Fig. 12, the SBH (Φ_{bo}) is defined as the potential difference between the Fermi level and the conduction band edge of GaN. However, the effective Φ_{bo} is influenced by some non-idealities such as image-force effect and surface states related to native oxide interface which can affect the semiconductors surface potential [33, 34].

Figure 13 denotes the current transport mechanism (CTM) in the forward-bias Au/Ta_2O_5/n-GaN MIS junction. The log (I) versus log (V) shows different linear regions (I, II, and III) yielding three different slopes. In Region-I, the calculated slope value is 1.68 which is close to unity indicating ohmic behaviour. The reason for this may be due to silicon doping to GaN and/or carriers which were created thermally [56]. The slope value estimated in the region-II was 5.63 which is higher than 2 may be attributable to the space-charge-limited current (SCLC) by way of presence of isolated trapping levels in GaN layer as well as in high-k Ta_2O_5 layer. When fitting was made in region-III, the value of slope decreases to 2.57 indicating that the prepared MIS SBD reaching the trap-filling limit [57, 58]. This analysis leads to the conclusion that there is clear transition in the carrier transport mechanism at the interfaces of Au/Ta_2O_5/n-GaN as a function of applied voltage.

To know the current conduction mechanisms that are taking place in the extracted reverse-bias I–V characteristics of the fabricated Au/Ta_2O_5/n-GaN MIS junction, ln (I_R) versus $V_R^{1/2}$ plot was made and is shown in Fig. 14. This plot allows one to know whether Poole–Frenkel emission (PFE) or Schottky emission (SE) conduction mechanisms is taking place in the extracted reverse-bias I–V curves of the fabricated device. In the reverse bias, if the current is dominated by PFE mechanism which can be expressed as [59]

$$I_R = I_o \exp\left(\frac{\beta_{PF} V^{1/2}}{kTd^{1/2}}\right), \tag{19}$$

and the SE mechanism is defined as

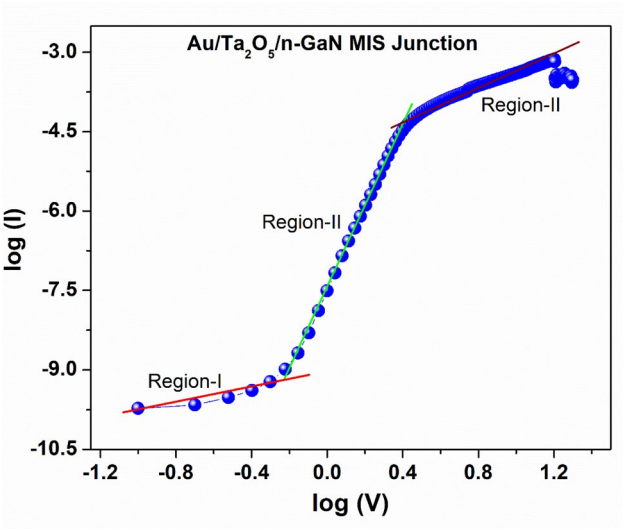

Fig. 13 The forward bias log (I) versus log (V) plot for the Au/Ta_2O_5/n-GaN MIS junction

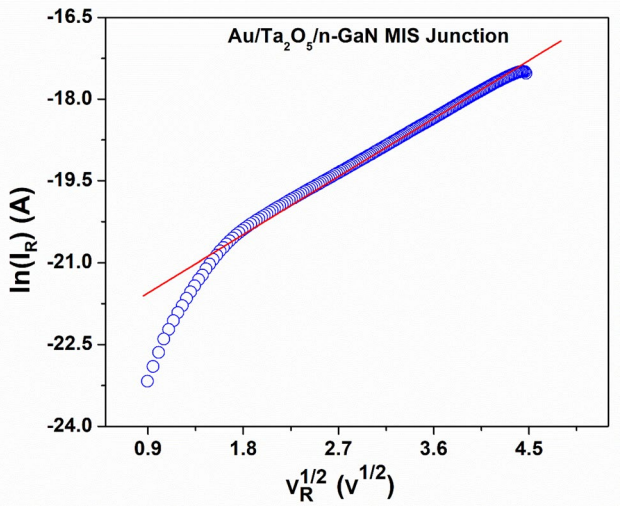

Fig. 14 Plot of ln (I_R) versus $V^{1/2}$ for the Au/Ta_2O_5/n-GaN MIS junction

$$I_R = AA^*T^2\exp\left(\frac{-\Phi_{bo}}{kT}\right)\exp\left(\frac{\beta_{SC}V^{1/2}}{kTd^{1/2}}\right), \tag{20}$$

where 'd' is the thickness of the film, β_{PF} is PFE and β_{SC} is SE field lowering coefficients, respectively. Further, the theoretical values for β_{PF} and β_{SC} can be written as

$$2\beta_{SC} = \beta_{PF} = \left(\frac{q^3}{\pi\varepsilon_o\varepsilon_r}\right)^{1/2}, \tag{21}$$

where q, ε_o and ε_r are the electric charge, relative permittivity of free space and semiconductor, respectively. Usually, the value of β_{PF} is twice the value of β_{SC}. The estimated theoretical values of β_{PF} and β_{SC} are 1.51×10^{-5} and 7.58×10^{-6} $eVm^{1/2}$ $V^{-1/2}$, respectively, for the Au/Ta_2O_5/n-GaN MIS SBDs. As shown in Fig. 14, the linear fitting in the plot of ln (I_R) versus $(V_R)^{1/2}$ confirms a linear relationship which demonstrate that the reverse current being dominated by PFE. The linear fitting to the ln (I_R) versus $(V_R)^{1/2}$ curve yielded the slope value of 4.54×10^{-5} $eVm^{1/2}$ $V^{-1/2}$ for the prepared MIS SBD. The experimentally calculated β_{PF} value of 4.54×10^{-5} $eVm^{1/2}$ $V^{-1/2}$ from the slope is approximately closer to the theoretical value calculated for PFE mechanism, i.e. 1.51×10^{-5} $eVm^{1/2}$ $V^{-1/2}$. Consequently, these results suggest that the PFE transport mechanism is governing the reverse leakage current in the prepared MIS SBD device. In the case of the PFE conduction mechanism, the theoretical and experimentally calculated values are not in very close agreements and this is due to the facts such as the existence of trap states in the bandgap of Ta_2O_5 insulating layer and structural defects with high density which enhances the trap levels/charge carriers de-trapping at the interfaces of the prepared MIS SBD devices [60, 61]. All the extracted Schottky barrier parameters using different methods from Figs. 4–14 were compared with the previously reported values in the literature [62–69] and tabulated in Table 2.

4 Conclusions

In summary, the Ta_2O_5 interlayer was deposited using e-beam evaporation technique onto n-type GaN. Electrical parameters of Au/Ta_2O_5/n-GaN MIS junctions have been discussed using I–V measurements with voltage range ± 20 V. Statistical distribution study was used to evaluate the average n and SBH values by fitting the Gaussian distribution function and the corresponding resulted values are 0.85 eV with a normal deviation of 0.00181 eV and 1.36 with normal deviation of 0.00562, respectively, for the MIS SBD heterojunction. The R_S and R_{Sh} values are also determined from I–V curves and the values are 4.2 kΩ and 3.81 GΩ, respectively. The electrical properties have been evaluated with diverse methods such as Rhoderick's, Cheung's, Modified Norde's, Hernandez's and Chattopadhyay's. The 'n' values are extracted using Cheung's and Chattopadhyay's method is close to unity (1), while this value is nearly > 2 by Rhoderick's and Hernandez's methods. The results revealed that the calculated SBH values obtained from forward bias I–V curves through different methods are almost consistent with each other. From the forward-bias I–V curves of Au/Ta_2O_5/n-GaN MIS junction, conduction mechanisms such as ohmic is found to be active in the low-voltage regime whereas SCLC at high voltage regimes, respectively. Furthermore, reverse I–V characteristics interpreted that PFE conduction mechanism is dominant in the fabricated Au/Ta_2O_5/n-GaN MIS heterojunction. To conclude, the betterment in rectification ratio, SBHs and good fitting of experimental data to equations of different methods were ascribed to the facts of deliberately deposited Ta_2O_5 and undoped GaN buffer layers in the fabricated Au/Ta_2O_5/n-GaN MIS SBD heterojunction.

Acknowledgements The author Dr. Nallabala Nanda Kumar Reddy thankfully acknowledge the financial support received from the Department of Science and Technology (DST), Science and Engineering Research Board, Government of India, Major Research Project No. ECR/2017/002868 and DST-FIST Program-2015 (SR/FST/College-263). Dr. C. Yuvaraj acknowledges the financial support received from TEQIP-II seed grant 2019-20. Dr. K. Venkata Krishnaiah is

Table. 2. Different Schottky barrier parameters acquired from the *I–V* characteristics of Au/Ta_2O_5/n-GaN MIS SBD in the present work and comparison with the previously reported MIS SBD structures in the literature

Barrier parameters	*I–V* measurements	statistical analysis average values	Cheung's functions d*V*/d(ln*I*) versus *I*	*H* (*I*) versus *I*	Norde plot	Ψ_S–*V* plot	Z (*V*, *T*)$_i$–*V* plot
Leakage current	1.467×10^{-10}		–	–	–	–	–
Barrier height (eV)	0.87 ± 0.01	0.85 ± 0.01	–	0.88 ± 2.0E-16	0.85 ± 0.01	0.82 ± 6E-17	0.89 ± 6E-4
Ideality factor (*n*)	1.29 ± 0.01	1.35 ± 0.01	1.30	–	–	1.28	1.32 ± 0.02
Series resistance (Ω)	4.2E3	–	22.6E3 ± 2.2E-12	19.7E3 ± 1.9E-12	96.2E6	–	–
Shunt resistance (Ω)	3.81E9	–	–	–	–	–	–

Comparison with the literature

Ref. no.	From *I–V*		Cheung's functions				Norde		Ψ_S–*V* plot		*Z*(*V*, *T*)$_i$–*V* plot	
			d*V*/d(ln*I*)-*I*		*H*(*I*)–*I*							
	Φ_{bo} (eV)	*n*	R_S	*n*	Φ_{bo} (eV)	R_S	Φ_{bo} (eV)	R_S	Φ_{bo} (eV)	*n*	$\Phi_{bo\ (eV)}$	*n*
[62]	0.63	1.3	–	–	–	–	–	–	–	–	–	–
[63]	–	3.12	27.9 k Ω	3.19	0.76	–	0.85	–	–	–	–	–
[64]	0.85	1.03	–	–	–	–	0.93	–	0.89	1.83	0.89	1.96
[65]	0.71	1.22	1.58 k Ω	1.31	0.30	1.41 k Ω	0.75	0.94 k Ω	0.71	1.22	0.76	1.24
[66]	0.36	3.86	42.9 Ω	4	0.41	4	0.44	42 Ω	0.40	3.65	0.39	4.5
[67]	0.80	1.39	436.8 k Ω	2.70	0.76	454 k Ω	0.79	14.2 MΩ	0.79	1.37	0.79	1.66
[68]	0.65	3.44	21.49 Ω	–	–	32.56 Ω	–	–	–	–	–	–
[69]	0.73	1.65	974.6 Ω	1.91	0.62	911 Ω	–	–	–	–	–	–

obliged to SERB-DST, New Delhi for sanctioning a major research project No. EMR/2017/000009. Further, all the authors thankful to the technical support received from Mr. G. Manjunatha, MITS, Madanapalle, A.P and Mr. Kewal Krishan, Department of Electronic Science, Kurukshetra University, India.

References

1. D.S. Lee, Z. Liu, T. Palacios, GaN high electron mobility transistors for sub-millimetre wave applications. Jpn. J. Appl. Phys. **53**, 100212 (2014)
2. S.J. Pearton, C. Kuo, GaN and related materials for device applications. MRS Bull. **22**, 17 (1997)
3. M.L. Gardner, *Master's Thesis* (Naval Postgraduate School, Monterey, USA, 2016).
4. Y. Chen, Z. Zhang, H. Jiang, Z. Li, G. Miao, H. Song, H. Liqin, T. Guo, Realization of an efficient electron source by ultraviolet-light-assisted field emission from a one-dimensional ZnO nanorods/n-GaN heterostructure photoconductive detector. Nanoscale. **11**, 1351 (2019)
5. Q. Zheng, C. Li, A. Rai, J.H. Leach, D.A. Broido, D.G. Cahill, Thermal conductivity of GaN, GaN, and SiC from 150 K to 850 K. Phys. Rev. Mater. **3**, 014601 (2019)
6. T.I. Kim, Y.H. Jung, J. Song, D. Kim, Y. Li, H. Kim, S. Song, J.J. Wierer, H. Pao, Y. Huang, J.A. Rogers, High-efficiency, microscale GaN light-emitting diodes and their thermal properties on unusual substrates. Small. **8**, 1643 (2012)
7. A.C. Schmitz, A.T. Ping, M.A. Khan, Q. Chen, J.W. Yang, I. Adesida, Schottky barrier properties of various metals on n-type GaN. Semicond. Sci. Technol. **11**, 1464 (1996)
8. P.T. Blanchard, K.A. Bertness, T.E. Harvery, L.M. Mansfield, A.W. Sanders, N.A. Sanford, MESFETs made from individual GaN nanowires. IEEE Trans. Nanotechnol. **7**, 760 (2008)
9. M.A. Khan, M.S. Shur, J.N. Kuznia, Q. Chen, J. Bourn, W. Schaff, Temperature activated conductance in GaN/AlGaN heterostructure field effect transistors operating at temperatures up to 300 °C. Appl. Phys. Lett. **66**, 1083 (1995)
10. S.J. Pearton, F. Ren, A.P. Zhang, G. Dang, X.A. Cao, K.P. Lee, H. Cho, B.P. Gila, J.W. Johnson, C. Monier, C.R. Abernathy, J. Han, A.G. Baca, J.-I. Chyi, C.-M. Lee, T.E. Nee, C.C. Chuo, S.N.G. Chu, GaN electronics for high power, high temperature applications. Mater. Sci. Eng. B **82**, 227 (2001)
11. N. Lakhdar, F. Djeffal, New optimized dual-material (DM) gate design to improve the submicron GaN-MESFETs reliability in subthreshold regime. Microelectron. Reliab. **52**, 958 (2012)
12. D. Voiry, H. Yamaguchi, J.W. Li, R. Silva, D.C.B. Alves, T. Fujita, M.W. Chen, T. Asefa, V.B. Shenoy, G. Eda, M. Chowalla, Enhanced catalytic activity in strained chemically exfoliated WS_2 nanosheets for hydrogen evolution. Nat. Mater. **12**, 850 (2013)
13. H.I. Karunadasa, E. Montalvo, Y. Sun, M. Majda, J.R. Long, C.J. Chang, A molecular MoS_2 edge site mimic for catalytic hydrogen generation. Science **335**, 698 (2012)
14. M.Y. Li, Y. Shi, C.-C. Cheng, L.-S. Lu, Y.-C. Lin, H.-L. Tang, M.-L. Tsai, C.-W. Chu, K.-H. Wei, J.-H. He, W.H. Chang, K. Suenaga, L.J. Li, Epitaxial growth of a monolayer WSe_2-MoS_2 lateral P-N junction with an atomically sharp interface. Science **349**, 524 (2015)
15. X. Xu, Z.Y. Fan, S.J. Ding, D.M. Yu, Y.P. Du, Fabrication of MoS_2 nanosheet @TiO_2 nanotube hybrid nanostructures for lithium storage. Nanoscale. **6**, 5245 (2014)
16. S.P. Murarka, Multilevel interconnections for ULSI and GSI era. Mater. Sci. Eng. R **19**, 87 (1997)

17. M.H. Tsai, S.C. Sun, C.E. Tsai, S.H. Chaung, H.T. Chiu, Comparison of the diffusion barrier properties of chemical-vapor-deposited TaN and sputtered TaN between Cu and Si. J. Appl. Phys. **79**, 6932 (1996)
18. M. Takeyama, A. Noya, T. Sase, A. Ohta, Properties of TaNx films as diffusion barriers in the thermally stable Cu/Si contact systems. J. Vac. Sci. Technol. B **14**, 674 (1996)
19. M.T. Wang, Y.C. Lin, M.C. Chen, Barrier properties of very thin Ta and TaN layers against copper diffusion. J. Electrochem. Soc. **145**, 2538 (1998)
20. T. Laurila, K. Zeng, J.K. Kivilahti, J. Molarius, T. Riekkinen, I. Suni, Tantalum carbide and nitride diffusion barriers for Cu metallisation. Microelectron. Eng. **60**, 71 (2002)
21. A.F. Jankowaski, R.M. Bionta, P.C. Gabriele, Internal stress minimization in the fabrication of transmissive multilayer x-ray optics. J. Vac. Sci. Technol. A **7**, 210 (1989)
22. K. Holloway, P.M. Fryer, Tantalum as a diffusion barrier between copper and silicon. Appl. Phys. Lett. **57**, 1736 (1990)
23. M. Oda, A. Ozawa, S. Ohki, H. Yoshihara, Ta film properties for X-ray mask absorbers. Jpn. J. Appl. Phys. **29**, 2616 (1990)
24. J.-H. Hur, M.-J. Lee, C.B. Lee, Y.-B. Kim, C.-J. Kim, Modeling for bipolar resistive memory switching in transition-metal oxides. Phy. Rev. B **82**, 155321 (2010)
25. M.-J. Lee, C.B. Lee, D. Lee, S.R. Lee, M. Chang, J.H. Hur, Y.-B. Kim, C.-J. Kim, D.H. Seo, S. Seo, U.-I. Chung, I.-K. Yoo, K. Kim, A fast, high-endurance and scalable non-volatile memory device made from asymmetric Ta2O($_{5-x}$)/TaO($_{2-x}$) bilayer structures. Nat. Mater. **10**, 625 (2011)
26. J.-H. Hur, K.M. Kim, M. Chang, S.R. Lee, D. Lee, C.B. Lee, M.-J. Lee, Y.-B. Kim, C.-J. Kim, U.-I. Chung, Modeling for multilevel switching in oxide-based bipolar resistive memory. Nanotechnology. **23**, 225702 (2012)
27. J. Yu, G. Chen, C.X. Li, M. Shafiei, J. Ou, J. du Plessis, K. Kalantar-zadeh, P.T. Lai, W. Wlodarski, Hydrogen gas sensing properties of Pt/Ta_2O_5 Schottky diodes based on Si and SiC substrates. Procedia Eng. **5**, 147 (2010)
28. S.-J. Joo, J.H. Choi, S.J. Kim, S.-C. Kim, Pd/Ta_2O_5/SiC Schottky-diode hydrogen sensors formed by using rapid thermal oxidation of Ta thin films. J. Korean Phys. Soc. **63**, 1794 (2013)
29. B.P. Lakshmi, V.R. Reddy, V. Janardhanam, M.S.P. Reddy, J.-H. Lee, Effect of annealing temperature on the electrical properties of Au/Ta_2O_5/n-GaN metal-insulator-semiconductor (MIS) structure. Appl. Phys. A. **113**, 713 (2013)
30. N. Alimardani, J.F. Conley Jr., Enhancing metal-insulator-insulator-metal tunnel diodes via defect enhanced direct tunnelling. J. Vac. Sci. Technol. A **105**, 082902 (2014)
31. N.N.K. Reddy, H.S. Akkera, M.C. Sekhar, S. Uthanna, Influence of Ta_2O_5 interfacial oxide layer thickness on electronic parameters of Al/Ta_2O_5/p-Si/Al. Silicon. **11**, 159 (2019)
32. S. Kumar, M.V. Kumar, S. Krishnaveni, Fabrication and analysis of the current transport mechanism of Ni/n-GaN Schottky barrier diodes through different models. Semicond. **54**, 169 (2020)
33. E.H. Rhoderick, R.H. Williams, *Metal-Semiconductor Contacts*, 2nd edn. (Clarendon, Oxford, 1988).
34. S.M. Sze, *Physics of Semiconductor Devices*, 2nd edn. (Wiley, New York, 1981).
35. N.N.K. Reddy, V.R. Reddy, C.-J. Choi, Electrical characteristics and interfacial reactions of rapidly annealed Pt/Ru Schottky contacts on n-type GaN. Phys. Status Solidi A **208**, 1670 (2011)
36. G. Zhang, Y. Xue, P. Guo, H. Wang, Z. Ma, Optical properties and microstructure of Ta_2O_5 thin films prepared by ion assisted electron beam evaporation. J. Wuhan Univ. Technol. Mat. Sci. Edit. **23**, 632 (2008)
37. R. Shakoury, S. Rezaee, F. Mwema, C. Luna, K. Ghosh, S. Jurecka, Ş Ţalu, A. Arman, A.G. Korpi, Multifractal and optical bandgap characterization of Ta_2O_5 thin films deposited by electron gun method. Opt. Quant. Electron. **52**, 95 (2020)
38. N.N.K. Reddy, S. Godavarthi, V.K. Kummara, K.M. Kumar, D. Saha, H.S. Akkera, G.K. Guntupalli, S. Kumar, S.V.P. Vattikuti, Structural, optical and photoresponse characteristics of metal-insulator-semiconductor (MIS) type Au/Ni/CeO_2/GaN Schottky barrier ultraviolet photodetector. Mater. Sci. Semicond. Process. **117**, 105190 (2020)
39. S. Kumar, M.V. Kumar, S. Krishnaveni, Fabrication and analysis of the current transport mechanism of Ni/n-GaN Schottky barrier diodes through different models. Semiconductors. **54**, 169 (2020)
40. M.C. Sekhar, N.N.K. Reddy, B.P. Reddy, B.P. Prakash, H.S. Akkera, S. Uthanna, S.H. Park, Influence of substrate bias voltage on crystallographic structure, optical and electronic properties of Al/(Ta2O5)$_{0.85}$(TiO2)$_{0.15}$/p-Si MIS schottky barrier diodes fabricated by dc magnetron sputtering. Mater. Sci. Semicond. Process. **76**, 80 (2018)
41. O. Akhavan, Silver nanocube crystals on titanium nitride buffer layer. J. Phys. D: Appl. Phys. **42**, 105305 (2009)
42. L. Dobos, B. Pecz, L. Toth, Z.J. Horvath, Z.E. Horvath, E. Horvath, A. Toth, B. Beaumont, Z. Bougrioua, Al and Ti/Al contacts on n-GaN. Vacuum **84**, 228 (2010)
43. M. Diserens, J. Patscheider, F. Levy, Improving the properties of titanium nitride by incorporation of silicon. Surf. Coat. Technol. **108–109**, 241 (1998)
44. J.M. Wang, W.G. Liu, T. Mei, The effect of thermal treatment on the electrical properties of titanium nitride thin films by filtered arc plasma method. Ceram. Int. **30**, 1921 (2004)
45. N. Chaturvedi, U. Zeimer, J. Würfl, G. Tränkle, Mechanism of ohmic contact formation in AlGaN/GaN high electron mobility transistors. Semicond. Sci. Technol. **21**, 175 (2006)
46. M.E. Lin, C. Ma, F.Y. Huang, Z.F. Fan, L.H. Allen, H. Morkoc, Low resistance ohmic contacts on wide band-gap GaN. Appl. Phys. Lett. **64**, 1003 (1994)
47. S. Kapoor, R. Laishram, H. Saini, S. Mahajan, R.K. Chaubey, D.S. Rawal, S. Vinayak, Effect of argon plasma treatment on ohmic contact formation in AlGaN/GaN HEMTs. Springer Proc. Phys. **215**, 191 (2019)
48. R.T. Tung, Electron transport at metal semiconductor interfaces: general theory. Phys. Rev. B **45**, 13509 (1992)
49. A.A.M. Farag, Influence of temperature and illumination on the characteristics of nanocrystalline $Ga_{0.29}$ $Al_{0.71}$As based heterojunction prepared by MOCVD. J. Alloys Compd. **509**, 8056 (2011)
50. S.K. Cheung, N.W. Cheung, Extraction of Schottky diode parameters from forward current-voltage characteristics. Appl. Phys. Lett. **49**, 85 (1986)
51. H. Norde, A modified forward I-V plot for Schottky diodes with high series resistance. J. Appl. Phys. **50**, 5052 (1979)
52. K.E. Bohlin, Generalized Norde plot including determination of the ideality factor. J. Appl. Phys. **60**, 1223 (1986)
53. M.P. Hernandez, C.F. Alonso, J.L. Pena, Barrier height determination in homogeneous nonideal Schottky contacts. J. Phys. D: Appl. Phys. **34**, 1157 (2001)
54. P. Chatopadhyay, A new technique for the determination of barrier height of Schottky barrier diodes. Solid-State Electron. **38**, 739 (1995)
55. J. Yu, G. Chen, C.X. Li, M. Shafiei, J.Z. Ou, J. du Plessis, K. Kalantar-zadeh, P.T. Lai, W. Wlodarski, Hydrogen gas sensing properties of Pt/Ta2O5 Schottky diodes based on Si and SiC substrates. Sens. Actuators A **172**, 9 (2011)
56. S. Kumar, M.V. Kumar, S. Krishnaveni, Fabrication and analysis of the current transport mechanism of Ni/n-GaN Schottky barrier diodes through different models. Semicond **54**, 169 (2020)

57. K. Ashish, V. Seema, R. Singh, Investigation of current-voltage characteristics of Ni/GaN schottky barrier diodes for potential HEMT applications. J. Nano-Electron. Phys. **3**, 671 (2011)
58. Y.S. Ocak, M. Kulakci, T. Kılıcoglu, R. Turan, K. Akkılıc, Current-voltage and capacitance-voltage characteristics of a Sn/methylene blue/p-Si Schottky diode. Synth. Met. **159**, 1603 (2009)
59. A.A. Kumar, V.R. Reddy, V. Janardhanam, H.D. Yang, H.-J. Yun, C.J. Choi, Electrical properties of Pt/n-type Ge Schottky contact with PEDOT:PSS interlayer. J. Alloys Compd. **549**, 18 (2013)
60. V.R. Reddy, V. Manjunath, V. Janardhanam, Y.-H. Kil, C.-J. Choi, Electrical properties and current transport mechanisms of the Au/n-GaN Schottky structure with solution-processed high-k $BaTiO_3$ interlayer. J. Electron. Mater. **43**, 3499 (2014)
61. R.M. Fleming, D.V. Lang, C.D.W. Jones, M.L. Steigerwald, D.W. Murphy, G.B. Alers, Y.-H. Wong, R.B.V. Dover, J.R. Kwo, A.M. Sergent, Defect dominated charge transport in amorphous Ta2O5 thin films. J. Appl. Phys. **88**, 850 (2000)
62. A. Shetty, B. Roul, S. Mukundan, L. Mohan, G. Chandan, K.J. Vinoy, S.B. Krupanidhi, Temperature dependent electrical characterisation of Pt/HfO_2/n-GaN metal-insulator-semiconductor (MIS) Schottky diodes. AIP Adv. **5**, 097103 (2015)
63. T.T.A. Tuan, D.H. Kuo, C.C. Li, W.C. Yen, Schottky barrier characteristics of Pt contacts to all sputtering-made n-type GaN and MOS diodes. J. Mater. Sci: Mater. Electron. **25**, 3264 (2014)
64. K. Akkılıc, Y.S. Ocak, T. Kılıcoglu, S. Ilhan, H. Temel, Calculation of current-voltage characteristics of a Cu (II) complex/n-Si/AuSb Schottky diode. Curr. Appl. Phys. **10**, 337 (2010)
65. S. Karatas, N. Yildirim, A. Turut, Electrical properties and interface state energy distributions of Cr/n-Si Schottky barrier diode. Superlattices Microstruct. **64**, 483 (2013)
66. I. Rahim, M. Shah, M. Iqbal, F. Wahab, A. Khan, S.H. Khan, Fabrication and electrical characterizations of graphene nanocomposite thin film based heterojunction diode. Phys. B **524**, 97 (2017)
67. R. Padma, G. Lee, J.S. Kang, S.C. Jun, Structural, chemical, and electrical parameters of Au/MoS_2/n-GaAs metal/2D/3D hybrid heterojunction. J. Colloid Interface Sci. **550**, 48 (2019)
68. A. Tataroglu, Comparative study of the electrical properties of Au/n-Si (MS) and Au/Si_3N_4/n-Si (MIS) Schottky diodes. Chin. Phys B. **22**, 068402 (2013)
69. O. Mustafa, Y. Fahrettin, Analysis of interface states and series resistance of Ag/SiO_2/n-Si MIS Schottky diode using current-voltage and impedance spectroscopy methods. Microelectron Eng **85**, 646 (2008)